High Shear Processing of Expanded Vermiculite Filled Polymer Composites: Particle Size Effect on Flexible Composites

MUKADDES SEVVAL CETIN[1,2], OZAN TOPRAKCI[1,2], OMER SUAT TASKIN[3], ABDULLAH AKSU[3] and HATICE AYLIN KARAHAN TOPRAKCI[1,2]*

[1]Department of Polymer Materials Engineering, Yalova, Turkey.
[2]Yalova University, Institute of Graduate Studies, Yalova, Turkey.
[3]Department of Chemical Oceanography, Institute of Marine Science and Management, Istanbul University, Istanbul, Turkey.

Abstract

Filler dispersion is an important issue for polymer-based composites. Fillers can be dispersed by melt or solution processing methods. Solution-based mixing offers various combinations including ultrasonication, mechanical stirring, or high shear mixing. Planetary high shear mixing is a simple method with high dispersion performance. Dispersion and wetting of the fillers are provided by not only planetary shear movement of the mixer but also by the decrease in viscosity of the polymer phase because of high shear. Although that is advantageous for the dispersion of nanofillers, it might be challenging for the particles that have morphology with loosely bonded layers. To observe the effects of high shear mixing on expanded vermiculite (VMT) filled styrene-[ethylene-(ethylene-propylene)]-styrene (SEEPS) flexible composites, two different VMTs were used with different particle sizes at various VMT ratios from 1 to 30 wt%. Morphological, structural, thermal, mechanical properties, flame spread character of the composites, and viscosity of the solutions were analyzed. From morphological analysis, high shear mixing was found to be effective in terms of decreasing particle size and filler dispersion. While mechanical properties showed decrease, thermal stability, and flame retardancy of the composites increased.

CONTACT Hatice Aylin Karahan Toprakci ✉ rohithitesh005@gmail.com ● Department of Polymer Materials Engineering, Yalova, Turkey.

Introduction

Styrene-[ethylene-(ethylene-propylene)]-styrene (SEEPS) is a styrenic thermoplastic elastomer (TPE). Basically it is a block copolymer with rigid styrene blocks and elastomeric ethylene-(ethylene-propylene) blocks. Styrene blocks function as hard segments those form physical cross-linking centers between elastomeric phase.[1–3] Because of so called physical-crosslinks, SEEPS is highly flexible with good recoverability and resilience those make it a promising material for various applications. It should also be mentioned that SEEPS is one of the most durable styrenic TPEs in terms of its high UV, weathering, and aging resistance. In addition to these, its high tensile strength, tensile strain and toughness make it unique for many applications including household appliances, adhesives, coatings, automotive parts.[1–3] It can be used as a compatibilizer[4,5] or a modifier[6,7] for binary or ternary blends with polypropylene (PP),[8] polyamide (PA),[9,10] polyethylene terephthalate (PET),[11] PP/polystyrene (PS),[6,7] PP/ground tire rubber.[4] In most of these studies, SEEPS amount and type were found significant in terms of blend properties. PP/SEEPS blends were reported to show lower elastic modulus and yield stress with higher level of tensile strain compared to PP.[8] Weng *et al.*, studied the rheological properties of the PA/SEEPS blends, and SEEPS ratio was found significant in terms of behavior and morphology.[9,12] In addition to binary blends, ternary blends of SEEPS were also reported in the literature. Lin *et al.* prepared recycled PET/SEEPS blends and investigated the addition of (maleic anhydride)-grafted-styrene-ethylene-butylene-styrene (SEBS-g-MAH) at different ratios on rheological, morphological, mechanical properties. As reported in the study, SEBS-g-MAH incorporation improved morphological, mechanical, rheological properties.[11] In another study, SEEPS was used as an interfacial modifier for PP/PS blends to fabricate membranes. PP/PS/SEEPS ratio, processing route, and conditions were found important for the membrane properties.[6,7] Application of SEEPS as a compatibilizer for PP/ground tire rubber blend was also investigated by Lu *et al*. Although various compatibilizers were used in the study, SEEPS was reported to show the highest performance for the interface properties between two phases.[4] In addition to SEEPS blends, there are couple of studies about the characterization of SEEPS mixtures with various oils.[13–15] From the recent literature given above, it is obvious that SEEPS is mostly used as a component of the polymeric systems. However, it can be used alone for the fabrication of fine fibers,[16] conductive polymer composites,[17] pressure sensors,[17] magnetorheological composites[18] with[18] or without extenders.[16,17] Polymeric composites are materials with improved properties those consist of at least one matrix and one filler. Incorporation of filler into the matrix leads to fabrication of functional materials. Various composites can be prepared from various sources.[19–23]

Vermiculite (VMT) is a multilayered natural inorganic material. Because of its nature, its content and structure might change based on the region and conditions. Depending on the structure and composition, various properties including density, hardness, delamination resistance, color, refractive index can change.[24–26] One of the most promising properties of VMT is its expandable structure results in an accordion-like porous particle morphology. This form of the VMT is called expanded vermiculite. As a result of expansion, distance between layers, porosity, surface area, and thermal resistance increase, density decreases and VMT becomes an important sustainable alternative filler for polymer composites. However, expanded layers are loosely bonded with low layer-layer interaction negatively affects the mechanical properties of VMT and it becomes sensitive to applied force including shear and compression. In order to make this disadvantage into an advantage, expanded vermiculites can be powdered by various methods in order to obtain different grades. By doing this size of the vermiculites can be tuned from couple of milimeters to nanometers.[24,26] In addition to this study, particle size was reported to be affected by processing conditions.[25] In order to investigate effects of processing conditions, two different VMT particles were used at various concentrations from[1-30] wt % with SEEPS matrix. Samples were prepared by a solution based high shear mixing and compression molding. Morphological, structural, thermal, mechanical properties, flame spread character of the composites and viscosity of the solutions were analyzed as a function of VMT type and concentration.

Material and Methods
Materials

Styrene-[ethylene-(ethylene-propylene)]-styrene block copolymer with 30% styrene content was used (SEPTON 4033, Kuraray Co Ltd.) as the matrix. Toluene (Merck) was used as the solvent. The raw VMT, with an average grain size of 250 mm, was kindly supplied from Karbosil Kimya Li. Co., Turkey. The company reported the wt% content of the VMT as: SiO_2 38-46, Al_2O_3 10-16, MgO 16-35, CaO 1-5, K_2O 1-6, FeO_3 6-13, TiO_2 1-3, H_2O 8-6, others 0.2-1.2. To obtain expanded VMT, a tube furnace (OTF-1200X, MTI) was used. The tube furnace was heated up to 900 ˚C after that sample was put into the furnace and kept at this temperature for 30 minutes. After this process, expanded VMT was powdered by using a mortar and a pestle. The samples were sieved and two different VMTs were obtained, and samples named as VMT-1 and VMT-2. As given in Fig. 1a and c, VMT-1 and VMT-2 had the average particle size value of 299.5 µm and 551.6 µm, respectively before the sample preparation.
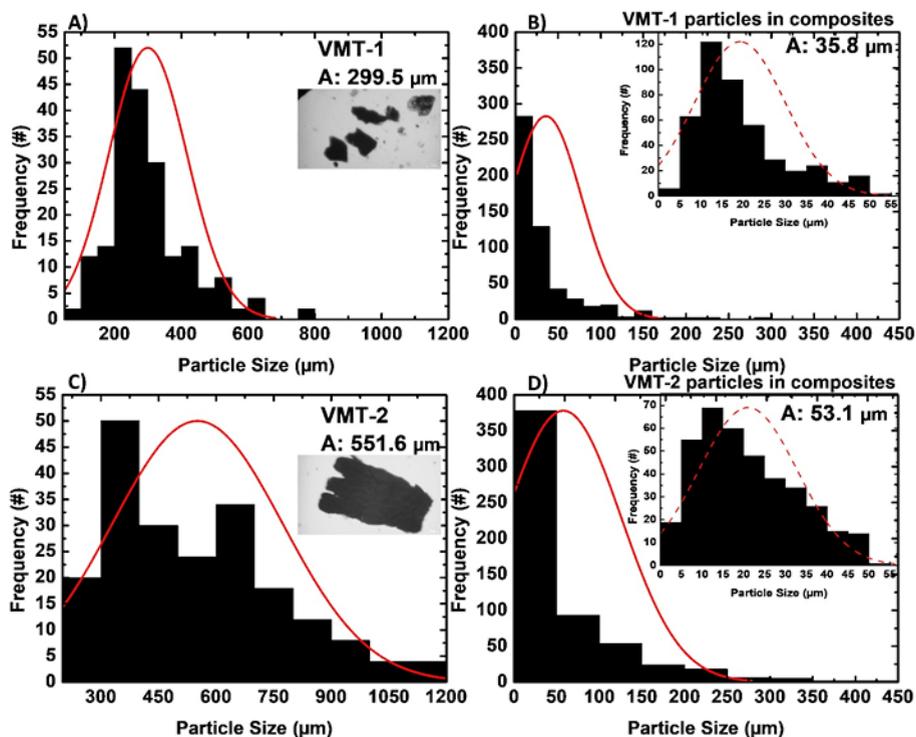

Fig. 1:Particle size distribution histogram of a) VMT-1, b) VMT-1 particles in composites (inset:d80), c) VMT-2, d) VMT-2 particles in composites (inset:d65), A:Avarage particle size (inset a, c: optical images of VMT-1 and VMT-2, respectively)

Preparation of the VMT/SEEPS Composites

The composites were prepared by combination of solvent casting and hot pressing. Before the process, VMT was dried in a vacuum oven (Wisd, WOV-20) for 15 h. at 80 °C. Toluene was used as a solvent and SEEPS, Toluene weight ratio was 1:3. Polymer was dissolved at 50 °C by a magnetic stirrer (Daihan MSH 20 D, 450 rpm). The weight % of the VMT was 1, 5, 10 and 20, 30 wt%. Preparation steps and digital images of the composites can be seen from Fig. 2. Since VMT has low density and high surface area with porous morphology, its interaction with the polymer might be challenging. To increase the interaction between VMTs and polymer and disperse the fillers homogeneously, a high shear mixer (Kurabo Mazerustar KK250, 1600 rpm) was used. Mixing was performed in two steps, in the first step VMT was mixed with the 2 g of solvent for a minute. In the second step, polymer solution was added and mixed under the same conditions.
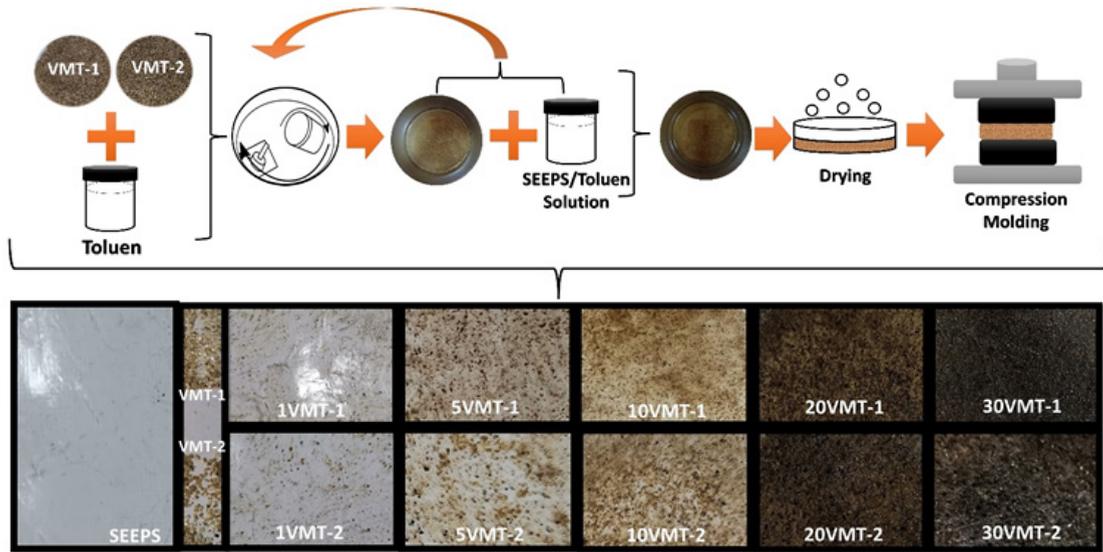
Fig. 2: Preparation steps and digital images of samples

Table 1: Sample codes, contents, viscosity and normalized viscosity values of the samples

Code	SEEPS Ratio (wt%)	Filler Type/ Filler Ratio (wt%)	Viscosity (cP)	Normalized Viscosity ($\eta/\eta SEEPS$,cP/cP)	Tensile Strength (MPa)/Tensile Strain (%)
SEEPS	100	-	1454	1	11.88/750.68
1VMT-1	99	VMT-1/1	1500	1.03	11.35/670.43
5VMT-1	95	VMT-1/5	1650	1.13	11.06/644.20
10VMT-1	90	VMT-1/10	1842	1.26	10.62/605.53
20VMT-1	80	VMT-1/20	2061	1.42	10.04/585.10
30VMT-1	70	VMT-1/30	2086	1.43	8.62/544.88
1VMT-2	99	VMT-2/1	1634	1.12	9.80/679.08
5VMT-2	95	VMT-2/5	1751	1.2	9.25/642.24
10VMT-2	90	VMT-2/10	2463	1.63	8.89/627.69
20VMT-2	80	VMT-2/20	2809	1.93	6.50/583.52
30VMT-2	70	VMT-2/30	2832	1.94	5.22/501.71

VMT/SEEPS/Toluene mixtures were cast into the Petri dishes. Samples were kept in an oven (Wisd, WOV-20) at 45 °C for 15 h to dry. In the next step solvent was further removed under vacuum at 80 °C for 15 h. To obtain homogeneous film morphology and film thickness, cast films were removed from the Petri dishes and compression molded (Gulnar Machine Laboratory type dual stage press) between teflon coated plates at 200 °C for 15 sec under 3 MPa following that composites were left to cool down at 25 ˚C for a minute.

Characterization of the Composites Morphological Analysis

To determine the average particle size of the VMT-1 and VMT-2 an optical microscope instrument (AmScope 40X-2500X LED) was used. Particle size distribution histograms were drawn based on the data obtained from by Image J. software. For the particle size, length and width of the particle were measured and average value was calculated. Field emission scanning electron microscopy (FESEM, 30 kV) was used for the analysis

of composite morphology. Composites were cut by a blade and Au/Pd alloy was used for the sputter coating (3-6 nm) on the sample cross-section before the analysis.

Viscosity

To observe the filler ratio and particle size on viscosity, VMT/SEEPS/toluene mixtures were analyzed by using Brookfield DV2T viscometer (USA). Sample weight was 7 g (5 g SEEPS/VMT/Toluene + 2 g Toluene) and characterization was performed at a speed of 200 rpm with a spindle number of #5 at room temperature (25°C, 60% RH). For each mixture three measurements were performed, and average values were reported (Extra 2 g of toluene was added into SEEPS solution before the measurement 5 g SEEPS/Toluene + 2 g Toluene). To compare the two sets, normalized viscosity (NV) was calculated from $_{\eta/\eta SEEPS}$, where η is the viscosity of the sample $_{\eta SEEPS}$ is the viscosity of the SEEPS solution.

Fourier Transform Infrared Spectroscopy (FTIR)

FTIR analysis was carried out by the attenuated total internal reflectance (ATR mode) spectroscopy (Perkin Elmer, Spectrum 100 IR spectrometer). Spectra were recorded in the transmittance mode between 650 and 4000 cm^{-1}, spectral resolution of 4 cm^{-1} at a scan rate of 4 scans.

Thermogravimetric Analysis (TGA)

To determine the thermal behavior of the SEEPS film and VMT/SEEPS composites, TGA analysis was carried out (Seiko, TG/DTA 6300) between 25 and 500 °C. Temperature was increased with the rate of 10 °C min^{-1} under 200 ml min-1 nitrogen flow rate.

Mechanical Characterization

Mechanical properties including tensile strength and tensile strain of SEEPS film, VMT-1/SEEPS and VMT-2/SEEPS composites were characterized by using a universal testing system (Devotrans, DVT GPU/RD). Samples were cut by a blade (length: width 15 mm: 5 mm). Before the test, the average thickness of the composites was determined by a thickness meter (Asimeto). Three tests were performed for each sample with the test speed of 100 mm/min.

Vertical Flame Spread Analysis

To compare the flame resistance of the samples, a simple flame spread analysis was performed. Samples were cut by a blade (length: 60 mm,width: 10 mm). Tests were carried out at 25 ˚C under 65% relative humidity. A metal ruler was placed on a stand and samples were attached on the ruler by a metal paper clip. Metal ruler was used in order to monitor the spread of the flame as a function of time. To start the flame adjustable kitchen lighter was used with same setting for all samples. The test was recorded by the video camera and to compare the flame retardancy of the samples, at different time intervals the images were captured from the video.

Results & Discussion
Morphological Analysis

1, 10, 20VMT-1 and 1, 10, 20VMT-2 composites were analyzed in terms of their microstructural morphology by considering behavior of polymer, filler size, filler geometry, filler orientation, filler distribution, filler-matrix interaction. As given in the cross-sectional SEM images (Fig. 3), SEEPS was the continuous phase and completely molten under given processing conditions and behaved as the binder between VMT particles for both sets. By increasing the VMT ratio, amount of the filler in the cross-section increased regardless of the VMT type. Those can be also confirmed by the digital images of the composites in Fig. 2. As obvious from the images, film formation was obtained for all samples and by increasing the filler concentration, samples turned into darker shade of brown. As seen from all SEM images (Fig. 3), the filler size in VMT-2 loaded composites were higher than VMT-1 loaded composites. As far as measured from the SEM images (Fig. 1b and d), approximate average size was determined as 35.8 and 53.1 µm for VMT-1 and VMT-2 loaded composites, respectively. However, the particle size observed in the composites were not same as in the particle size distribution histograms. As mentioned previously, before the sample preparation, average particle size values were determined as 299.5 and 551.6 µm for VMT-1 and VMT-2, respectively. The decrease in particle size could be an indication of separation of VMT layers from the surface of the particles or breakdown of VMT particles and that was assumed to be caused by expanded VMT morphology and composite processing conditions.
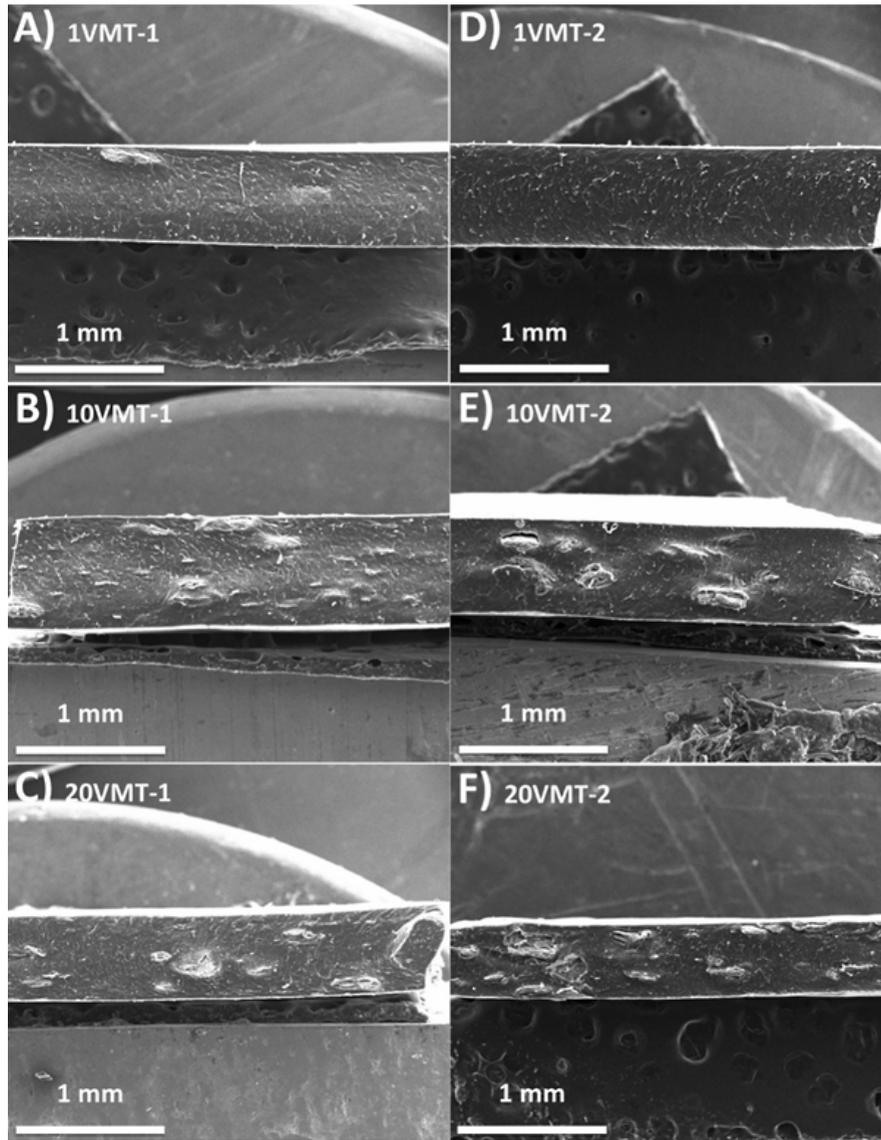
Fig. 3: SEM images of composites a) 1VMT-1, b) 10VMT-1, c) 20VMT-1 d) 1VMT-2, e) 10VMT-2, and f) 20VMT-2

As known, vermiculite has a multilayered morphology. During expansion process, morphology turns into a curved, accordion-like structure. The layers expand and loosely bind to each other. When the morphology of the VMTs is considered in the SEEPS phase, basically two different morphologies were observed. For both composites, multilayered, accordion-like large particles and a few layered small particles can be observed from Fig. 3 and 4.

As mentioned in the composite preparation, filler was dispersed both in the solvent and in the polymer solution by a planetary high-shear mixer. As observed previously[27] and reported in the literature,[28] high shear mixing led to change in the morphology of VMT particles. To observe such effects SEM images taken at higher magnifications were given in Fig. 4, and as obvious from the images, a few-layer thick sheets separated from the outer surface and dispersed in

the SEEPS matrix regardless of the particle size. When the composites were analyzed in terms of filler orientation, particle morphology was found significant. While larger particles with multilayered morphology tended to align parallel to the film axis (Fig. 3), same behavior was not observed for a few layered VMTs (Fig. 4). The orientation of the larger particles probably caused by the fabrication method. As previously mentioned in the methods section, compression molding under 3MPa probably led to alignment of VMTs parallel to the film axis.[29,30] On the other hand, during high-shear mixing, smaller particles dispersed in the SEEPS matrix without any orientation and applied pressure was not sufficient for the dominant orientation. Fig. 4 can also be used to observe the filler-matrix interface and void formation for both fillers. As obvious from the images,

loosely bounded outer layers of VMTs separated from the surface and formed a few layered VMTs and they were well-wetted and dispersed in the SEEPS matrix with a good interface. However, the inner body of VMTs could not interact with the matrix and voids were formed at the boundary between a few layered VMTs and inner body of VMTs. That was assumed to be caused by not only separation of a few layered VMTs but also processing conditions. Under pressure and thermal energy, molten SEEPS matrix wetted the surface of VMT. When the pressure is removed, relaxation of SEEPS phase probably led to separation of loosely bonded outer layersand void formation (Fig. 4).The void content was found to be higher at higher filler loading.In addition to these, at higher filler loading, VMTs tend to form agglomerates.
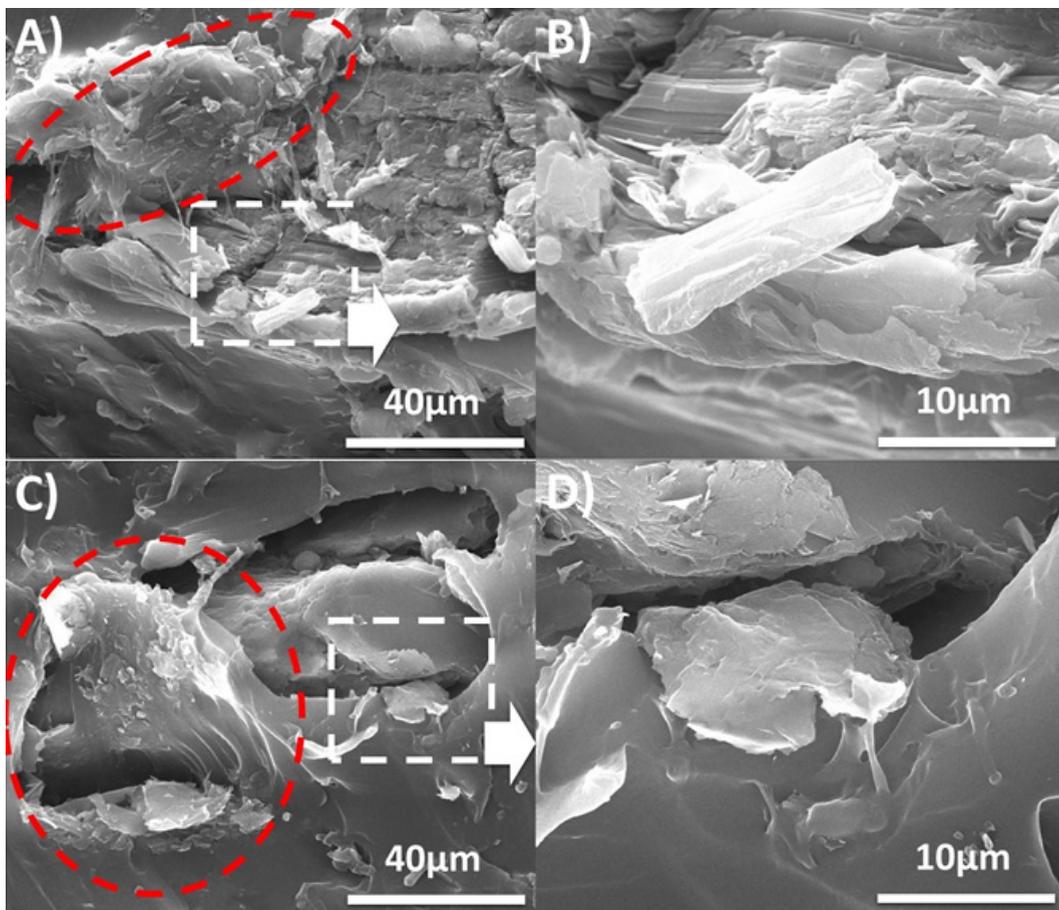

**Fig. 4:SEM images that show the few layer VMTs separated from the particle
a) 20VMT-1 at 2.5kx, b) 20VMT-1 at 10kx, c) 20VMT-2 at 2.5kx, and d) 20VMT-2 at 10kx**

Viscosity

Viscosity and normalized viscosity values of the samples can be seen from Table 1 and Fig. 5 as a function of VMT loading ratio. As seen from Fig. 5, viscosity of the samples increased parallel with the filler ratio regardless of the VMT type. VMT restricted the flow ability of the polymer solution because of its rigid structure. The viscosity values of SEEPS, 1, 5, 10, 20, 30VMT-1 were measured as 1454, 1500, 1650, 1842, 2061, 2086 cP, respectively. The NV values were calculated as 1.03, 1.13, 1.26, 1.42, 1.43 for 1, 5, 10, 20, 30VMT-1, respectively. The viscosity values of 1, 5, 10, 20, 30VMT-2 were measured as 1634, 1751, 2463, 2809, 2832 cP, respectively. The NV values were calculated as 1.12, 1.2, 1.63, 1.93, 1.94 for 1, 5, 10, 20, 30VMT-

2, respectively. As obvious from the outcomes, in all cases VMT-2 filled samples showed higher viscosity. That was assumed to be caused larger particle size. However, while at 1 and 5 wt% filler loading, the viscosity values were close for VMT-1 and VMT-2, the difference showed an increasing trend from 10 wt% filler loading. As given in Fig. 5b, both sets showed percolative behavior in terms of viscosity change. However, VMT-2 filled set showed a drastic change in viscosity between 5 and 10 wt% filling ratio that is defined as rheological percolation at which filler-filler interaction and resistance to flow increased. The highest viscosity values were obtained for 30VMT-1 and 30 VMT-2 those showed around 43% and 94% increase in viscosity, respectively.
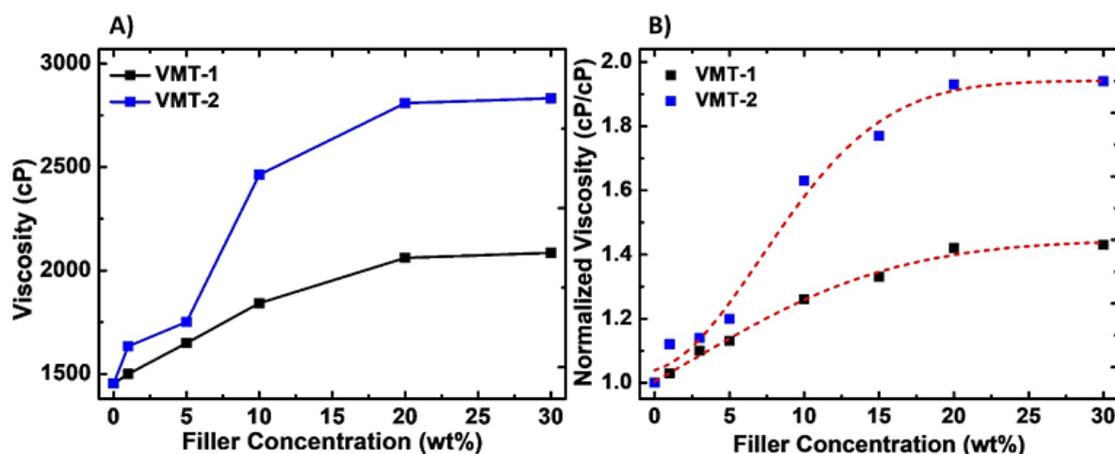

Fig. 5: a) Viscosity and b) normalized viscosity values of the samples

FTIR Analysis

FTIR analysis of the 10 and 20VMT-1/2 filled composites and SEEPS film can be seen from Fig. 6. FTIR peaks related with styrenic unit of styrene-[ethylene-(ethylene-propylene)]-styrene block copolymer can be seen at 697 and 756 cm^{-1}. These peaks were corresponded to bending aromatic ring of C-H. Also, the band between 1450 and 1500 cm^{-1} was associated with stretching aromatic ring of C-C[31]. The peak at 1376 cm^{-1} was corresponded to symmetrical bending vibrations of –C-H (CH3). The peak observed at 2950 cm^{-1} was an asymmetric stretching belonging to the CH3 group, whereas CH3 observed at 1456 cm^{-1} had a symmetrical bending type peak of the repeating units

of ethylene-(ethylene-propylene). The characteristic peaks related with asymmetric stretching vibrations of –C-H (CH2) can be seen at 2850 and 2920 cm-1[32]. Peaks between 800-1160 cm^{-1} were caused by peaks connected to the C-C groups of the block copolymer.[27,32,33]

Since results of the vermiculites were commonly similar, only one infrared spectrum was given as VMT-1/2. Vermiculite showed a few weak to medium intensity bands, and their positions vary with the amount of inorganic content distribution accordingly. All VMT/SEEPS composites showed similar trend, but the width of Si-O band was different in various specimens possibly due to the difference in the

range of their particle size distribution. In addition to that, for VMT/SEEPS composites, as shown in the inset image, characteristic transmission % intensity between 900–1100 cm^{-1} was observed to increase parallel with the concentration and particle size of VMT.[34,35]
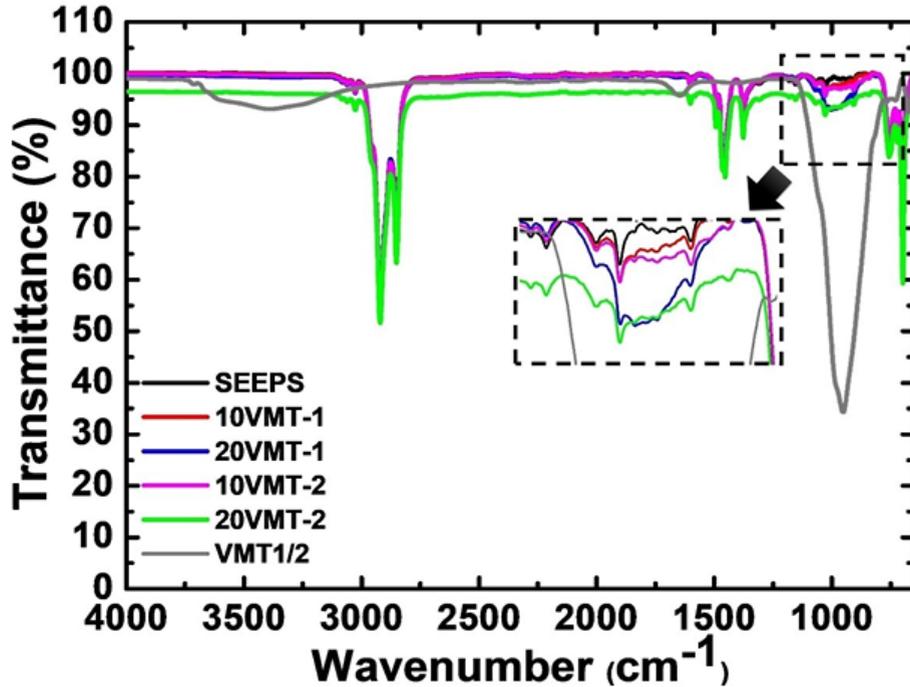

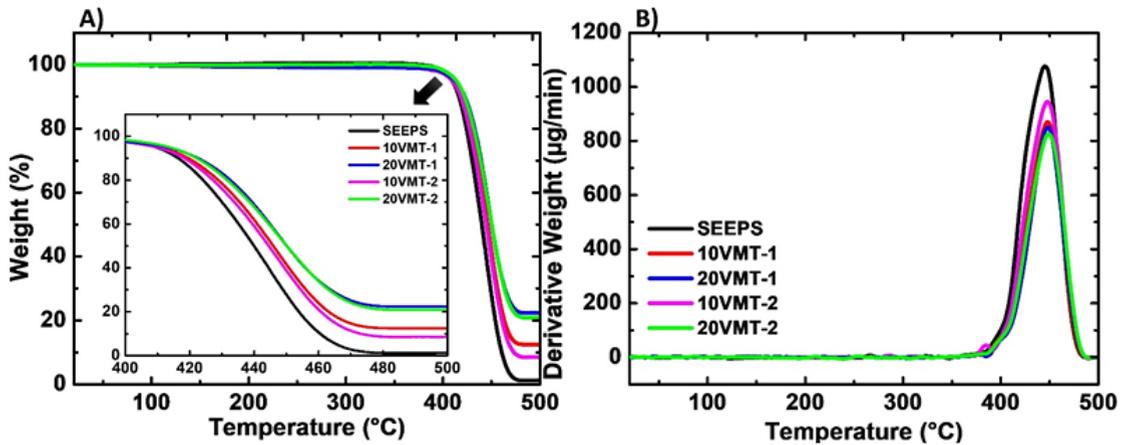**Fig. 6: FTIR results of VMT, SEEPS and VMT/SEEPS composites**

Fig. 7:a) TGA and b) DTG curves of the SEEPS film, 10, 20VMT-1, and 10, 20VMT-2 composites

Thermal Gravimetric Analysis
Thermal degradation behavior between 25-500 ˚C for the SEEPS film and composites can be seen in Table 2 and Fig.7. SEEPS showed thermal stability up to 400 ˚C. As given in Table 2, T10% and T50% values were determined as 416 ˚C and 439 ˚C, respectively. The char % was determined as 1.5. As known, vermiculite is a thermally stable mineral

that can stand high temperatures.[27] Based on this fact, it was expected to observe increase in thermal stability after addition of VMTs into the SEEPS. Regardless of the VMT type, thermal stability and char yield increased. At 20 wt% VMT concentration stability and char yield was higher compared to 10 wt% VMT filled composites. No significant difference was observed between VMT-1 and VMT-2 in terms of their contribution to thermal stability.

Table 2: Thermal degradation behavior of the SEEPS film and VMT/SEEPS composites

Sample	T10% (°C)	T50% (°C)	$T_{max\ degredation}$ (°C)	Weight Loss $T_{max\ degredation}$ (%)	Char Yield (%)
SEEPS	416.37	439.85	445.22	61.73	1.47
10wt%VMT-1/ SEEPS	418.37	445.92	447.95	54.19	12.59
10wt%VMT-2/ SEEPS	418.48	444.48	447.85	56.76	8.89
20wt%VMT-1/ SEEPS	422.50	450.01	448.36	46.50	22.51
20wt%VMT-2/ SEEPS	422.06	449.98	448.98	47.92	21.1

Mechanical Characterization

Tensile stress-strain graphs of SEEPS film and composites can be seen from Fig. 8 and averaged values can be seen from Table 1. The tensile strength of SEEPS, 1, 5, 10, 20, 30VMT-1 were measured as 11.88, 11.35, 11.06, 10.62, 10.04, 8.62 MPa, respectively. Increase in VMT-1 loading ratio led to decrease in tensile strength. Parallel with this conclusion, VMT-2 loaded composites also showed decreasing trend in terms of tensile strength. The values were determined as 9.80, 9.25, 8.89, 6.50, 5.22 MPa for 1, 5, 10, 20, 30VMT-2, respectively. Although both VMTs led to decrease in mechanical resistance to break, VMT-2/SEEPS composites showed lower values compared to VMT-1/SEEPS composites. That kind of response probably caused by filler-matrix interaction as explained in morphology analysis section. During film formation, samples exposure to thermal energy and compressive force to melt SEEPS matrix. Although, molten SEEPS wetted the surface of VMTs, after the removal of compressive force, relaxation of SEEPS phase probably led to separation of loosely bonded, a few layered outer layers from the VMT body (Fig. 4). As a consequence of that, filler-matrix interface and mechanical resistance to break were negatively affected. That was also reflected as a decrease in strain at break values as shown in Fig.9. Regardless of the VMT type, increase in VMT concentration led to decrease in tensile strain values. SEEPS, 1, 5, 10, 20, 30VMT-1 had tensile strain values as 750, 670, 644, 605, 585, 544 %, respectively. The tensile strain values of 1, 5, 10, 20, 30VMT-2 were measured as 679, 642, 627, 583, 501 %, respectively. Unlike in tensile strength, no significance difference was observed between two sets.
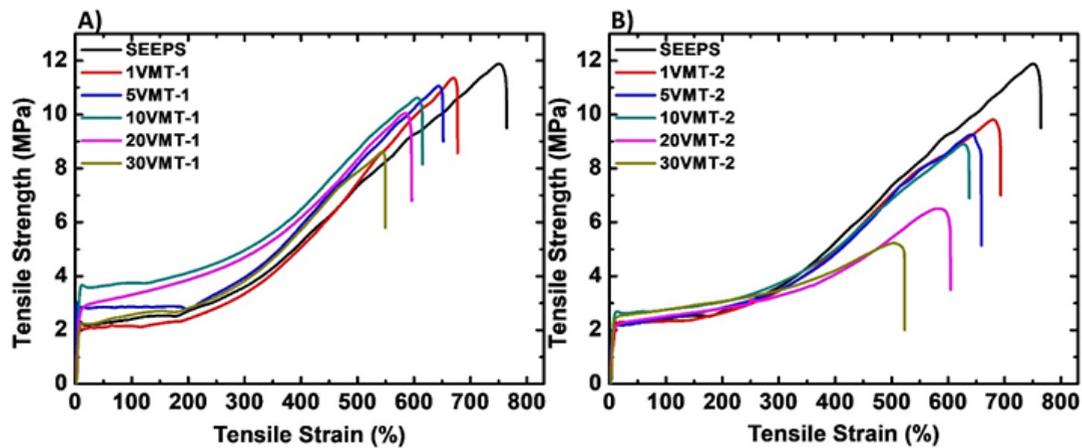

Fig. 8:Stress strain graphs of a) VMT-1/SEEPS and b) VMT-2/SEEPS composites
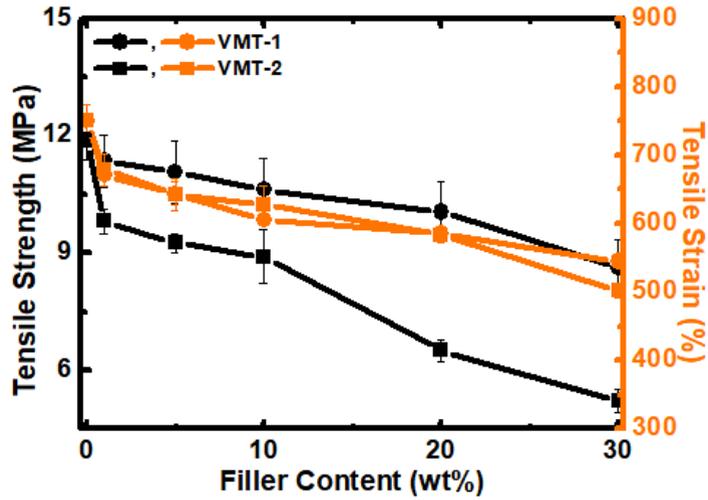
Fig. 9: Tensile strength and tensile strain values of the composites as a function of filler ratio

Vertical Flame Spread Analysis

Vertical flame spread analysis is a simple way of observing flame resistance of the materials. SEEPS is a hydrocarbon-based styrenic block copolymer with high flammability. In this work, flame was started, and tests were recorded by a video camera (Supplementary material, Video 1) and to compare the flame spread behavior of the samples, images were captured for 5, 10, 30VMT-1 and 5, 10, 30VMT-2 composites at different time intervals based on their performance. As shown in Fig. 10, by increasing the VMT ratio, flame resistance of the samples increased for both sets.
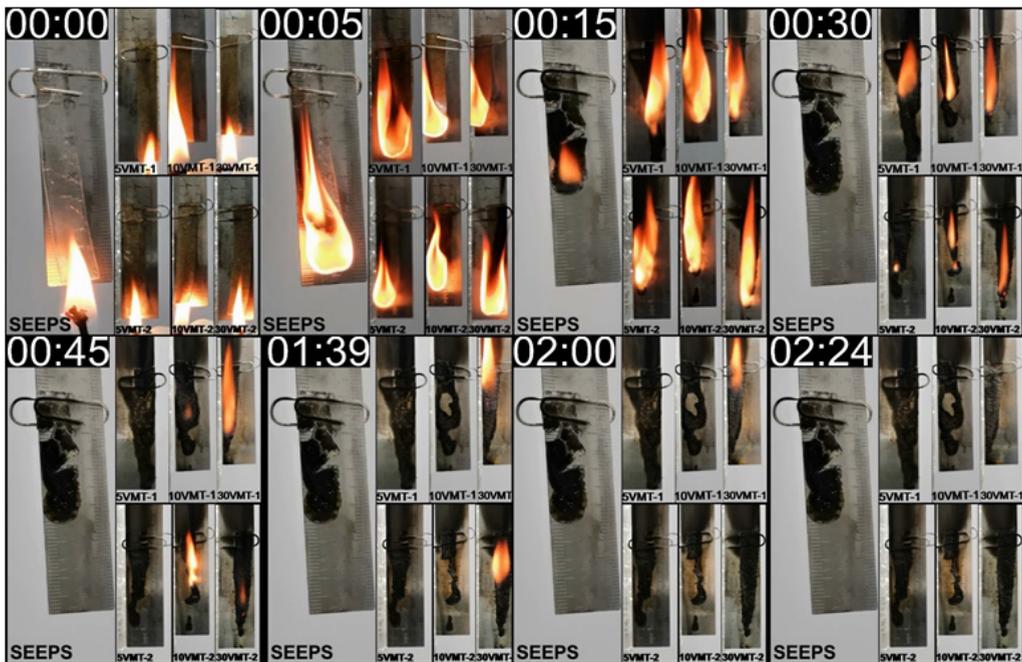

Fig. 10:Flame spread test results for 5, 10, 30VMT-1, and 5, 10, 30VMT-2

The samples were evaluated in terms of burning behavior, time required for complete burning and residual char morphology. The digital images of samples before and after test were given in Fig. 11. For SEEPS film, thermal degradation and melting took place together as in thermoplastics and dripping of the residual char/molten polymer mixture was observed. SEEPSfilm shrank vertically as soon as test started. Burning completed around 20 sec. and residual char was a black rigid solid as given in Fig. 11. Similar burning behavior was observed for 1, 5VMT-1 and 1, 5VMT-2 samples. However, 5VMTs showed slower shrinkage, and bended during burning test. The burning stopped after 43 and 33 sec. for 5VMT-1 and 5VMT-2, respectively. Residual char was foamy rigid solid. 10VMT-1 and 10VMT-2 showed less dripping and less shrinkage and bending compared to 5VMTs. The required time for complete burning was 49 and 99 sec. for 10VMT-1 and 10VMT-2, respectively. Residual char showed higher porosity compared to 5VMTs. 20, 30VMT-1 and 20, 30VMT-2 showed almost best performance in terms flame retardancy. For 30VMTs both films showed high thermal dimensional stability and less dripping. The total time was 144 and 100 sec. for 30VMT-1 and 30VMT-2, respectively. The residual char was bulky foam and easily crumbled in the hand. In addition to these VMT containing samples burned with a shiny glow.
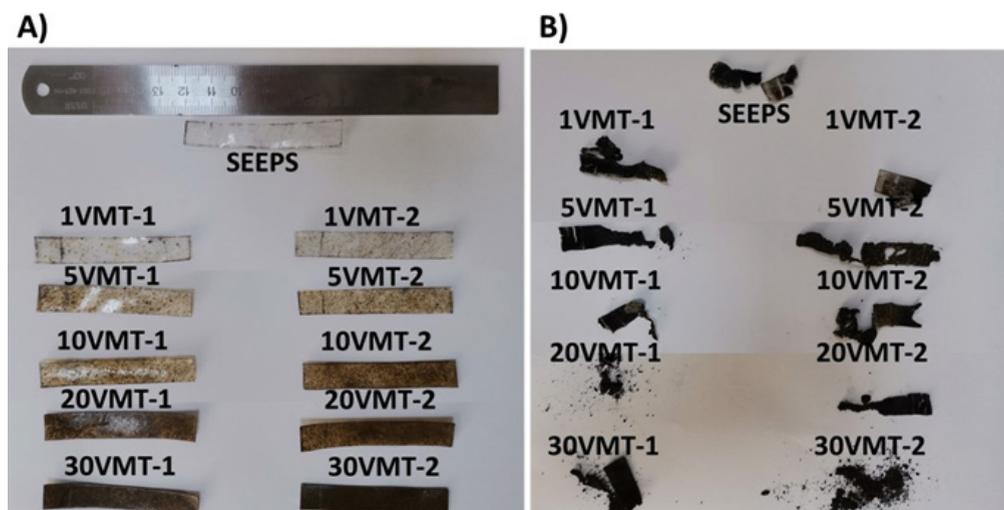

Fig. 11:Samples a) before and b) after the flame spread test

The flame retardancy of VMT was previously reported in many studies, but none of these studies flame retardancy performance was evaluated based on the filler size. As can be seen from the results and supplementary material, Video 1, VMT-1 generally showed higher performance in terms of flame retardancy. That was probably caused by better dispersion of smaller particles in the SEEPS matrix. The mechanism of flame retardancy of VMT was previously studied and reported by many authors.[27,36–43] One of the most important reasons for flame retardancy is the composition of the VMT. SiO_2, $Al2O_3$, MgO, Fe_2O_3 are the common components of VMT. SiO_2[44,45] $Al_2O_{3,45}$ $MgO,_{46–51}$ and Fe_2O_3[52] were reported to have high thermal stability and improve the thermal stability, flame retardancy and smoke suppression of the polymeric composites. The flame retardancy mechanism was not only attributed to VMT composition but also residual foam formation during burning.[27,36–43,50,51] In addition to thermal insulation capacity and oxygen barrier property of VMT, formation of multi-layered, foamy, carbon-based char formation with good heat and oxygen prevention capacity led to increase in spread of flame during the test.

Conclusions

In this study, expanded vermiculite filled SEEPS composites were reported for the first time in the literature. High shear mixing was used to disperse VMT particles in the matrix. In order to investigate

the effects of high shear mixing on composite properties, two different fillers were prepared from the same batch as VMT-1 (299.5 µm) and VMT-2 (551.6 µm). Filler concentration was between 1-30 wt%. Parallel with the starting size, VMT-2 filled composites showed higher particle size in the SEM images. However, as far as measured from the SEM images approximate average size was determined as 35.8 and 53.1 µm for VMT-1/SEEPS and VMT-2/SEEPS composites. That was caused by removal of loosely bonded a few layered particles from VMTs by the effect of high shear mixing. Solution viscosity of VMT loaded samples showed increase with the VMT incorporation. FTIR analysis showed that fillers were homogeneously dispersed throughout the SEEPS matrix. Although mechanical properties of the composites showed a decreasing trend for both sets, VMT-2/SEEPS showed higher decrease in tensile strength and strain. Thermal stability and flame retardancy of the composites improved with the VMT addition and VMT-1/SEEPS composites showed better performance. This study work is of importance not only for fabrication of SEEPS based flexible polymeric composites but also for VMT processing and final size distribution of VMT in the polymer composites. For the fabrication of VMT filled polymer composites, processing conditions should be considered for the final properties and performance of the materials. The composites prepared in this work can be used as flexible, stretchable flame-retardant coatings for various substrates such as protective clothing, home-textiles and geotextiles so future work will focus on these applications.

Conflict of Interest
We declare that there is no conflict of interest regarding the research work carried out and the publication of this article.

References

1. Wang X,Wu S,Wang K. Thermal Analysis Kinetics of the Chemical Crosslinking Reaction of the Styrene-Based Block Copolymer SEEPS. *Curr Phys Chem* 2011;1 (1): 65–68. doi:10.2174/1877946811101010065.

2. Wang W,Zheng Q,Yu Q. Study on the Viscoelastic Behavior of SEEPS Block Copolymer Based on a Modified BSW Model. *Chinese Science Bulletin* 2005;50 (19): 2171–2175. doi:10.1360/982005-132.

3. Zheng Q,Wang W,Yu Q,Yu J,He L,Tan H. Nonlinear Viscoelastic Behavior of Styrene-[Ethylene-(Ethylene-Propylene)]- Styrene Block Copolymer. *J Polym Sci B Polym Phys* 2006;44 (9): 1309–1319. doi:10.1002/polb.20772.

4. Lu Y,Yang Y,Xiao P,Feng Y,Liu L,Tian M,Li X,Zhang L. Effect of Interfacial Enhancing on Morphology, Mechanical, and Rheological Properties of Polypropylene-Ground Tire Rubber Powder Blends. *J Appl Polym Sci* 2017;134 (40): 45354. doi:10.1002/APP.45354.

5. Wu J. The Interfacial Properties and Porous Structures of Polymer Blends Characterized by Synchrotron Small-Angle X-Ray Scattering. *Polymer (Guildf)* 2003;44 (26): 8033–8040. doi:10.1016/j.polymer.2003.09.059.

6. Xanthos M,Chandavasu C,Sirkar KK,Gogos CG. Melt Processed Microporous Films from Compatibilized Immiscible Blends with Potential as Membranes. *Polym Eng Sci* 2002;42 (4): 810–825. doi:10.1002/PEN.10993.

7. Chandavasu C,Xanthos M,Sirkar KK,Gogos CG. Fabrication of Microporous Polymeric Membranes by Melt Processing of Immiscible Blends. *J Memb Sci* 2003;211 (1): 167–175. doi:10.1016/S0376-7388(02)00032-7.

8. Alanalp MB,Durmus A. Quantifying Microstructural, Thermal, Mechanical and Solid-State Viscoelastic Properties of Polyolefin Blend Type Thermoplastic

Elastomer Compounds. *Polymer (Guildf)* 2018;142: 267–276. doi:10.1016/j. polymer.2018.03.054.

9. Wang W,Lu Z,Cao Y,Chen J,Wang J,Zheng Q. Investigation and Prediction on the Nonlinear Viscoelastic Behaviors of Nylon1212 Toughened with Elastomer. *J Appl Polym Sci* 2012;123 (3): 1283–1292. doi:10.1002/APP.34624.

10. Wang W,Cao Y,Wang J,Zheng Q. The Gelation Behaviors of the Reactive Blends of Nylon1212 and Functional Elastomer. *J Mater Sci* 2008;43 (17): 5755–5762. doi:10.1007/s10853-008-2885-6.

11. Lin X,Qian Q,Xiao L,Huang Q,Zhou W,Chen Q,Zhang H. Melt Rheology and Properties of Compatibilized Recycled Poly(Ethylene Terephthalate)/(Styrene-Ethylene-Ethylene-Propylene-Styrene) Block Copolymer Blends. *Journal of Vinyl and Additive Technology* 2016;22 (3): 342–349. doi:10.1002/vnl.21450.

12. Wang W,Shangguan Y,Zhao L,Yu J,He L,Tan H,Zheng Q. The Linear Viscoelastic Behaviors of Nylon1212 Blends Toughened with Elastomer. *J Appl Polym Sci* 2008;108 (3): 1744–1754. doi:10.1002/app.27266.

13. Takahashi R,Nishioka A,Ishigami A,Suzuki T,Nishitsuji S,Koda T,Aoki Y. Rheology of Polystyrene-Block-Poly[Ethylene-Co-(Ethylene-Propylene)]-Block-Polystyre Ne Tri-Block Copolymer/Paraffinic Oil Blends - Effect of Oil Molecular Weight on the Order-Disorder Transition. *Nihon Reoroji Gakkaishi* 2012;40 (4): 171–177. doi:10.1678/rheology.40.171.

14. Aoki Y,Takahashi R,Nishitsuji S,Ishigami A,Koda T,Nishioka A. Viscoelasticity and Morphology of Polystyrene-Block-Poly[Ethylene-Co-(Ethylene-Propylene)]-Block-Polystyrene Tri-Block Copolymer/Paraffinic Oil Blends. 1. Effect of Oil Content. *Rheol Acta* 2016;55 (4): 293–301. doi:10.1007/s00397-016-0917-8.

15. Nishioka A,Aoki Y,Suzuki T,Ishigami A,Endo T,Koda T,Koyama K. Dynamic Mechanical Properties of Polystyrene-Block-Poly[Ethylene-Co- (Ethylene-Propylene)]-Block-Polystyrene Triblock Copolymer/Hydrocarbon Oil Blends. *J Appl Polym Sci* 2011;121 (5): 3001–3006. doi:10.1002/app.33923.

16. Toprakci O,Cetin MS,Karahan Toprakci HA. Production of Styrene-[Ethylene-(Ethylene-Propylene)]-Styrene Block Copolymer (SEEPS) Microfibers by Electrospinning. *Material Science Research India* 2021;18 (1): 27–36. doi:10.13005/msri/180104.

17. Karahan Toprakci HA,Turgut A,Toprakci O. Flexible Composites Used as Piezoresistive Pressure Sensors. *Mater Today Proc* 2021;46: 6904–6907. doi:10.1016/J.MATPR.2021.01.555.

18. Li W,Qiao X,Lu X,Chen J,Gong X,Yang T,Sun K,Chen X,Li W. Microstructure and Magnetorheological Properties of the Thermoplastic Magnetorheological Elastomer Composites Containing Modified Carbonyl Iron Particles and Poly(Styrene-b-Ethylene-Ethylenepropylene-b-Styrene) Matrix. *Smart Mater Struct* 2012;21 (11): 115028. doi:10.1088/0964-1726/21/11/115028.

19. Kumar RP,Muthukrishnan M,Sahayaraj AF. Experimental Investigation on Jute/Snake Grass/Kenaf Fiber Reinforced Novel Hybrid Composites with Annona Reticulata Seed Filler Addition. *Mater Res Express* 2022;9 (9): 095304. doi:10.1088/2053-1591/ac92ca.

20. Jenish I,Sahayaraj AF,Suresh V,Mani raj J,Appadurai M,Irudaya Raj EF,Nasif O,Alfarraj S,Kumaravel AK. Analysis of the Hybrid of Mudar/Snake Grass Fiber-Reinforced Epoxy with Nano-Silica Filler Composite for Structural Application. *Advances in Materials Science and Engineering* 2022;2022: 7805146. doi:10.1155/2022/7805146.

21. Sahayaraj AF,Muthukrishnan M,Ramesh M,Rajeshkumar L. Effect of Hybridization on Properties of Tamarind (Tamarindus Indica L.) Seed Nano-Powder Incorporated Jute-Hemp Fibers Reinforced Epoxy Composites. *Polym Compos* 2021;42 (12): 6611–6620. doi:https://doi.org/10.1002/pc.26326.

22. Felix Sahayaraj A,Muthukrishnan M,Ramesh M. Influence of Tamarindus Indica Seed Nano-Powder on Properties of Luffa Cylindrica (L.) Fruit Waste Fiber Reinforced Polymer Composites. *Polym Compos* 2022;43 (9): 6442–6452. doi:https://doi.org/10.1002/pc.26957.

23. Hariprasad P,Kannan M,Ramesh C,Felix Sahayaraj A,Jenish I,Hussain F,Khedher N

ben,Boudjemline A,Suresh V. Mechanical and Morphological Studies of *Sansevieria Trifasciata* Fiber-Reinforced Polyester Composites with the Addition of SiO2 and B4C. *Advances in Materials Science and Engineering* 2022;2022: 1634670. doi:10.1155/2022/1634670.

24. Suvorov SA,Skurikhin V V. Vermiculite - A Promising Material for High- Temperature Heat Insulators. *Refractories and Industrial Ceramics* 2003;44 (3): 186–193. doi:10.1023/A:1026312619843.

25. Toprakci O,Cetin MS,Toprakci Karahan HA. Vermiculite Filled Polymer Composites. In *Theory and Research in Engineering* II; 2020; Vol. 1, pp 125–144.

26. Raviv M,Lieth JH,Bar-Tal A. *Soilless Culture: Theory and Practice*; 2019; doi:10.1016/C2015-0-01470-8.

27. Cetin MS,Toprakci O,Taskin OS,Aksu A,Toprakci HAK. Expanded Vermiculite-Filled Flexible Polymer Composites: *Journal of Elastomers & Plastics* 2022;54 (1): 145–168.

28. Janica I,Del Buffa S,Mikołajczak A,Eredia M,Pakulski D,Ciesielski A,Samorì P. Thermal Insulation with 2D Materials: Liquid Phase Exfoliated Vermiculite Functional Nanosheets. *Nanoscale* 2018;10 (48): 23182–23190. doi:10.1039/c8nr08364a.

29. Buessem WR. The Mechanism of the Deformation of Clay. *Clays Clay Miner* 1953;2 (1): 480–491. doi:10.1346/ccmn.1953.0020138.

30. Balima F,Le Floch S,San-Miguel A,Reinert L,Duclaux L,Nguyen AN,Daniel I,Brûlet A,Gremillard L,Pischedda V. Porosity Evolution of Expanded Vermiculite under Pressure: The Effect of Pre-Compaction. *SN Appl Sci* 2019;1 (6):. doi:10.1007/s42452-019-0627-9.

31. Kumar Y,Singh SK,Oberoi D,Kumar P,Mohanty P,Ravindranath SS. Effect of Molecular Structure and Concentration of Styrene-Butadiene Polymer on Upper Service Temperature Rheological Properties of Modified Binders. *Constr Build Mater* 2020;249: 118790. doi:10.1016/j.conbuildmat.2020.118790.

32. Setyaningrum DL,Riyanto S,Rohman A. Analysis of Corn and Soybean Oils in Red Fruit Oil Using FTIR Spectroscopy in Combination with Partial Least Square. *Int Food Res J* 2013;20 (4): 1977–1981.

33. Asandulesa M,George R,Topala I,Pohoata V,Dobromir M,Dumitrascu N. Poly (Ethylene Glycol-Co-Styrene) Films Deposited by Plasma Polymerization Reactions at Atmospheric Pressure. *The Open Plasma Physics Journal* 2013;6 (1): 14–18. doi:10.2174/1876534301306010014.

34. El-Nemr KF,Ali MAM,Hassan MM,Hamed HE. Synergistic Effect of Vermiculite Clay and Ionizing Irradiation on the Physical and Mechanical Properties of Polybutadiene Rubber/Ethylene Propylene Diene Monomer Nanocomposite. *Radiochim Acta* 2019;107 (3):. doi:10.1515/ract-2018-3035.

35. Chung O,Jeong SG,Kim S. Preparation of Energy Efficient Paraffinic PCMs/Expanded Vermiculite and Perlite Composites for Energy Saving in Buildings. *Solar Energy Materials and Solar Cells* 2015;137: 107–112. doi:10.1016/j.solmat.2014.11.001.

36. Yan L,Fu L,Chen Y,Tian H,Xiang A,Rajulu AV. Improved Thermal Stability and Flame Resistance of Flexible Polyimide Foams by Vermiculite Reinforcement. *J Appl Polym Sci* 2017;134 (20): 44828. doi:10.1002/app.44828.

37. Wang F,Gao Z,Zheng M,Sun J. Thermal Degradation and Fire Performance of Plywood Treated with Expanded Vermiculite. *Fire Mater* 2016;40 (3): 427–433. doi:10.1002/fam.2297.

38. Xiong W,Wu J,Tian H,Xiang A,Wang C,Wu Q. Enhanced Mechanical and Thermal Properties of Polyurethane-Imide Foams with the Addition of Expended Vermiculite. *Polym Compos* 2020;41 (3): 886–892. doi:10.1002/pc.25419.

39. Kumar SP,Takamori S,Araki H,Kuroda S. Flame Retardancy of Clay-Sodium Silicate Composite Coatings on Wood for Construction Purposes. *RSC Adv* 2015;5 (43): 34109–34116. doi:10.1039/c5ra04682c.

40. Szadkowski B,Marzec A,Rybinski P,Zukowski W,Zaborski M. Characterization of Ethylene-Propylene Composites Filled with Perlite and Vermiculite Minerals: Mechanical, Barrier, and Flammability Properties. *Materials* 2020;13 (3): 585. doi:10.3390/ma13030585.

41. Cheong JY,Ahn J,Seo M,Nam YS. Flame-

Retardant, Flexible Vermiculite-Polymer Hybrid Film. RSC *Adv* 2015;5 (76): 61768–61774. doi:10.1039/c5ra08382f.

42. Macheca AD,Focke WW,Kaci M,Panampilly B,Androsch R. Flame Retarding Polyamide 11 with Exfoliated Vermiculite Nanoflakes. *Polym Eng Sci* 2018;58 (10): 1746–1755. doi:10.1002/pen.24775.

43. Chen S,Wang B,Kang J,Chen J,Gai J,Yang L,Cao Y. Synergistic Effect of Organic Vermiculite on the Flame Retardancy and Thermal Stability of Intumescent Polypropylene Composites. *Journal of Macromolecular Science, Part B: Physics* 2013;52 (9): 1212–1225. doi:10.1080/0022 2348.2012.760392.

44. Hribernik S,Smole MS,Kleinschek KS,Bele M,Jamnik J,Gaberscek M. Flame Retardant Activity of SiO2-Coated Regenerated Cellulose Fibres. *Polym Degrad Stab* 2007;92 (11): 1957–1965. doi:10.1016/j.polymdegradstab.2007.08.010.

45. Periadurai T,Vijayakumar CT, Balasubramanian M. Thermal Decomposition and Flame Retardant Behaviour of SiO 2-Phenolic Nanocomposite. *J Anal Appl* Pyrolysis 2010;89 (2): 244–249. doi:10.1016/j.jaap.2010.08.010.

46. Zheng T,Xia W,Guo J,Wang K,Zeng M,Wu Q,Liu Y. Preparation of Flame-Retardant Polyamide 6 by Incorporating MgO Combined with g-C3N4. *Polym Adv Technol* 2020;31 (9): 1963–1971. doi:10.1002/pat.4920.

47. Akram MW,Fakhar-E-Alam M,Atif M,Butt AR,Asghar A,Jamil Y, Alimgeer KS, Wang ZM. In Vitro Evaluation of the Toxic Effects of MgO Nanostructure in Hela Cell Line. *Sci Rep* 2018;8 (1):. doi:10.1038/s41598-018-23105-y.

48. Zhan Z,Shi J,Zhang Y,Zhang Y,Zhang B,Liu W. The Study on Flame Retardancy Synergetic Mechanism of Magnesium Oxide for PA66/AlPi Composite. *Mater Res Express* 2019;6 (11): 115317. doi:10.1088/2053-1591/ab4737.

49. Ma ZL,Fan CR,Lu GY,Liu XY,Zhang H. Synergy of Magnesium and Calcium Oxides in Intumescent Flame-Retarded Polypropylene. *J Appl Polym Sci* 2012;125 (5): 3567–3574. doi:10.1002/app.36227.

50. Zaharuddin WAW,Ariwahjoedi B,Hussain P. Effect of Vermiculite Addition on Thermal Characteristic of Water-Based Acrylic Fire Retardant Coating Formulation. *Journal of Applied Sciences* 2011;11 (10): 1763–1769. doi:10.3923/jas.2011.1763.1769.

51. Ribeiro SPS,Estevão LRM,Nascimento RSV. Brazilian Clays as Synergistic Agents in an Ethylenic Polymer Matrix Containing an Intumescent Formulation. *In Journal of Thermal Analysis and Calorimetry*; 2007; Vol. 87, pp 661–665. doi:10.1007/s10973-006-7872-z.

52. Mei N,Mingshuo Z,Baoxiaa X,Ruihonga Q,Mingqianga S,Li Z. Introducing the Fe2O3 Particles into Fiber for Flame Retardancy and Smoke Suppression. *The Journal of The Textile Institute* 2022; doi:https://doi.org/10.1 080/00405000.2022.2026580.